Food Research International 80 (2016) 12–18

Contents lists available at ScienceDirect

Food Research International

journal homepage: www.elsevier.com/locate/foodres

The bubble size distribution and its evolution in non-yeasted wheat flour doughs investigated by synchrotron X-ray microtomography

Filiz Koksel [a], Serdar Aritan [b], Anatoliy Strybulevych [c], John H. Page [c], Martin G. Scanlon [a,*]

[a] Food Science Department, University of Manitoba, Winnipeg, MB, Canada
[b] Biomechanics Research Group, Faculty of Sports Sciences, Hacettepe University, Ankara, Turkey
[c] Physics and Astronomy Department, University of Manitoba, Winnipeg, MB, Canada

ARTICLE INFO

Article history:
Received 4 August 2015
Received in revised form 4 December 2015
Accepted 5 December 2015
Available online 8 December 2015

Keywords:
X-ray microtomography
Synchrotron source
Bubble size distribution
Bread dough
Disproportionation
Bubble dynamics

ABSTRACT

Determination of the bubble size distribution at the end of mixing and controlling its changes are the basis for improving bread quality before it is fully manufactured. X-rays from a synchrotron source (Biomedical Imaging and Therapy beamline, Canadian Light Source) were used to rapidly characterize the bubble size distribution and its evolution in non-yeasted dough subsamples as a function of time for 3 h following mixing. A complete X-ray microtomography scan was completed within 120 s. The higher number density of bubbles in dough compared to results previously reported in the literature was attributed to the better contrast and higher resolution (smaller pixel size, 8.75 μm) of the reconstructed X-ray images generated from synchrotron X-rays. The bubble size distribution was very well characterized with a lognormal distribution function. This distribution had a median bubble radius of 22.1 ± 0.7 μm at 36 min after the end of mixing which increased to 27.3 ± 0.7 μm over 162 min, a trend indicative of transport of gas in the dough due to disproportionation. This is the first time disproportionation in non-yeasted wheat flour doughs has been monitored directly under bulk conditions relevant to dough in bakery conditions. These results show that the diffusion-driven dynamics of bubbles in non-yeasted bread doughs can be followed by X-rays from a synchrotron source via feature extraction using image analysis software.

1. Introduction

In breadmaking, starting with the mixing process, bubbles in dough are manipulated both in number and size (Campbell, Herrero-Sanchez, Payo-Rodriguez, & Merchan, 2001; Campbell, Rielly, Fryer, & Sadd, 1998; Koksel & Scanlon, 2012). Control of the bubble population in dough during mixing is crucial not only because no new air bubble nuclei are created for subsequent bubble growth during later stages of breadmaking (Baker & Mize, 1941), but also because dough aeration affects the rheological properties of the dough (Chin, Martin, & Campbell, 2005; Scanlon, Elmehdi, Leroy, & Page, 2008) and the cellular structure of the loaf created from the dough (Campbell et al., 1998; Chin & Campbell, 2005a). Therefore, determination of the bubble size distribution (BSD) at the end of mixing, and monitoring how it changes with time, are essential for controlling final loaf quality, especially for mechanically developed doughs (Chin & Campbell, 2005b). Furthermore, beyond the obvious technological application of the results, dough is a perfect candidate material for investigating time-dependent changes in bubble-laden foods and other aerated materials since it is a moderately stable soft solid allowing gas exchange for extended periods of time while not allowing the bubbles to cream out of the dough matrix.

In doughs made both with and without yeast, air bubbles are occluded as a significant volume fraction during the mixing process (Campbell et al., 1998; Koksel & Scanlon, 2012; Koksel, Strybulevych, Page, & Scanlon, 2014); the distribution of these bubbles is subject to significant changes over time. In non-yeasted doughs, the primary mechanism driving change in the BSD is disproportionation. Disproportionation occurs because gas diffuses from small bubbles to adjacent larger ones due to greater Laplace pressures in the smaller bubbles (Kokelaar, van Vliet, & Prins, 1996; Murray & Ettelaie, 2004; Shimiya & Nakamura, 1997; Shimiya & Yano, 1988). The wide range of bubble sizes in wheat flour doughs created by mixing has the consequence that smaller bubbles tend to shrink and disappear while the larger ones tend to grow (van Vliet, 1999).

Despite the importance of knowledge of the distribution of bubble sizes in dough, the literature is not replete with studies. Evaluation of the microstructure of dough is challenging because dough is opaque, and the bubbles in dough are extremely fragile and they change very rapidly (Bellido, Scanlon, Page, & Hallgrimsson, 2006; Scanlon et al., 2008, 2011; Shimiya & Nakamura, 1997; Strybulevych et al., 2012). One technique that can cope with opacity and fragility is the non-invasive method, X-ray microtomography. X-ray microtomography has been

* Corresponding author.
E-mail address: scanlon@cc.umanitoba.ca (M.G. Scanlon).

http://dx.doi.org/10.1016/j.foodres.2015.12.005
0963-9969/

widely used and is very well-suited for scrutinizing the three dimensional (3D) structure of bread and other stable cellular food products (Babin, Della Valle, Dendievel, Lourdin, & Salvo, 2007; Falcone et al., 2006; Trater, Alavi, & Rizvi, 2005). Coping with the rapid dynamics of the BSD in dough requires the more powerful X-rays of a synchrotron source to accurately capture the complexity of the 3D morphology of bread dough rapidly. As a result, the evolution of the 3D bubble microstructure of bread dough during fermentation has been achieved by the use of synchrotron X-ray radiation (Babin et al., 2006, 2008; Turbin-Orger et al., 2015, 2012).

Understanding dough aeration and the dynamics of the BSD can shed light on the mechanisms by which the final loaf texture is attained, and how the aerated structure of the final loaf can be improved as early as the mixing stage. It can also elucidate gas exchange mechanisms in aerated hydrated soft solid materials. Given the effectiveness of X-ray radiation from a synchrotron source, the objectives of this study were to determine the BSD in non-yeasted doughs and to quantify the time-dependent changes of the BSD in these doughs. Thus, we report the first quantitative assessment of disproportionation dynamics in this soft, viscoelastic material.

2. Materials and methods

2.1. Materials and sample preparation

All purpose wheat flour (13.0% moisture, 11.7% protein) was purchased locally (Rogers Food Ltd., no additive, unbleached, Armstrong, BC, Canada). Moisture content and protein content (Nx5.7) were determined according to Approved Method 44-15.02 and Approved Method 46-13 (AACC International, 2010) using a Kjeldahl 1002 distilling unit (Tecator, Prabin and Co. AB, Klippan, Sweden), respectively. The water absorption of the flour was determined to be 68% by Farinograph (Farinograph/Resistograph, FA-R/2, Duisburg, Germany) using Approved Method 54-21.01(AACC International, 2010).

The dough samples, with a composition of 200 g wheat flour, 68% distilled water and 2.4% salt (on fwb), were mixed for 3.5 min using a pin mixer (116 rpm) (National MFG. Co., Lincoln, NE, USA). The mixer had a 200 g mixing bowl, which was connected to a water circulation unit (Haake C with Haake C3 cooling unit, Berlin, Germany) set at 16 °C in order to produce a dough at room temperature (23 ± 0.5 °C) at the end of mixing.

To prepare a dough subsample for the X-ray microtomography tests, a pathology blade was used to excise a cylindrical dough subsample of approximately 1–1.5 cm diameter from the center of the dough immediately after mixing. The dough subsample was gently placed in a cylindrical plastic container and the lid of the plastic container was closed in order to prevent moisture loss. The container and the dough subsample were immediately mounted on the rotation stage within the experimental hutch (at 21 ± 1.0 °C) of the X-ray beamline.

2.2. Experimental methods

The 3D structure of the dough subsamples was characterized on the Biomedical Imaging and Therapy beamline (BMIT-BM 05B1-1) at the Canadian Light Source (Saskatoon, SK), using a filtered white beam with a peak beam energy of 18 keV. For filtering of the beam, aluminum filters (thicknesses of 0.200 mm, 0.883 mm and 2.500 mm) and a molybdenum filter (thickness of 0.200 mm) were inserted in the beamline. Preliminary experiments were performed so that the scanning procedure was optimized. As a result, the distance between the detector and the dough subsample was selected as 1.47 m, and the distance between the detector and the source was 26.2 m. The beam size was 40 mm (horizontal) by 5 mm (vertical). The detector was an AA-60 beam monitor (Hamamatsu C9300-124) with 8.75 μm/pixel resolution at the scintillator. Before X-ray data acquisition of dough samples, two different reference scans were performed to eliminate noise effects. These two references are: (1) no sample holder and no transmission of X-rays, (2) with X-ray transmission but without the sample holder in the experimental hutch of the beamline.

The sample scanning procedure comprised rotation through 180° at a rotation speed of 1.500°/s, with an exposure time of 200 ms/radiograph which allowed the acquisition of a complete scan of over 180° within 120 s. As a result, 350 serial cross-sectional 2530 × 2530 pixel^2 grayscale images were produced from radiographs of each microtomography scan. Bubble dynamics were monitored over the course of 3 h (a new scan every 2 min for the first 90 min and then a new scan every 10 min for a further 90 min). Three replicate doughs were prepared and one dough subsample from each dough replicate was tested by X-ray microtomography. Two stacks, each of 100 slices, were analyzed from two different locations within each dough subsample for each scan time.

Quantitative 3D features (bubble size distribution and its time evolution) were determined by image analyses performed with custom written programs in a MATLAB environment. Image analyses started with selection of a representative elementary area from the center of the 2D images to minimize any edge effects caused by sample cutting. Intensities of the 2D images were improved by using an image enhancement technique. This technique, which utilizes a 'histogram equalization' method in MATLAB, transforms the intensity plot of an original image into a new intensity plot with a new range of intensities. As a result, the new range of intensities conformed to a flat histogram with 64 bins. After increasing the contrast with the use of this image enhancement technique, a threshold value was chosen so that these high contrast grayscale images were binarized by replacing all pixels greater than the threshold value with white (bubbles) and the rest of the pixels with black (dough matrix). When choosing the threshold value, images were processed in such a way that the volume fraction of gas determined by X-ray analyses (ϕ_{X-ray}) was equivalent to that determined by density measurements ($\phi_{density}$) at the time when the density measurements were performed (approximately 15 min after the end of mixing). Dough density measurements and gas volume fraction based on density measurements ($\phi_{density}$) were performed according to Koksel and Scanlon (2012) and Koksel et al. (2014), respectively. For all other times, the thresholding settings were kept the same as the settings used for the time corresponding to density measurements. Finally, quantification of the 3D features was pursued by bubble tracking based on a 6-point neighboring 3D connectivity criterion over the stacks of 2D images (Kaufman, Cohen, & Yagel, 1993; Vu, Rangayyan, Deglint, & Boag, 2007).

Characterization of the BSD and its evolution was performed with Igor Pro data analysis and graphics software using its built-in lognormal distribution function (Igor Pro, WaveMetrics, Inc., Lake Oswego, OR). The reported BSD at a specific time after mixing was the average BSD obtained from both stacks (each of 100 slices) from three dough replicates except for scans performed at 76, 106, 120, 176 and 190 min after the end of mixing, where only 2 dough replicates were available. The frequency distributions of bubble sizes were constructed from discrete bubble sizes by grouping bubbles into 25 size classes (1, 2, 3, 4, 5, 10 or 30 μm wide) in total, depending on bubble numbers of a given range in a stack.

3. Results and discussion

3.1. Bubble size distributions

One 2D cross-sectional X-ray microtomography image (165 × 147 pixel^2, pixel size = 8.75 μm), and its binarized and segmented image, for a non-yeasted dough subsample tested 36 min after the end of mixing are represented in Fig. 1a and b, respectively. The 2D cross-sectional image allows for identification of the dough matrix (gray) and bubbles (black), with bubble cross-sections generally appearing to be circular (Fig. 1a and b). The 3D volume element

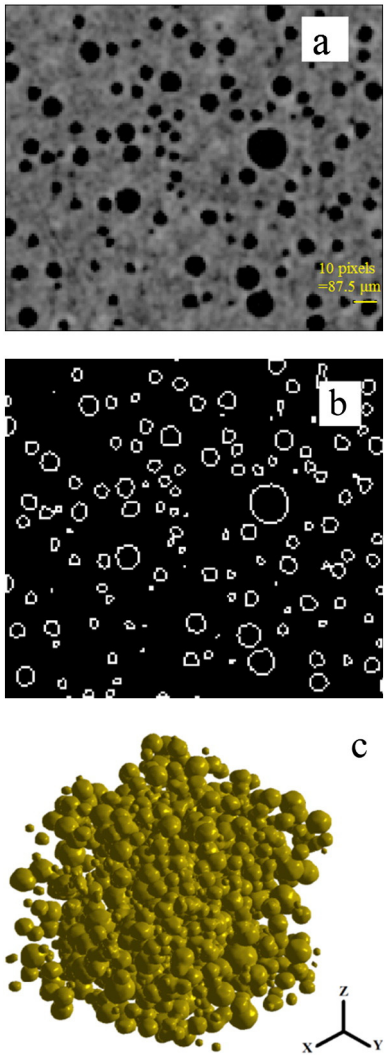

Fig. 1. (a) A 2D cross-sectional X-ray microtomography image of a non-yeasted dough subsample tested 36 min after the end of mixing, black: bubble cross-sections, gray: dough matrix; (b) the binarized and segmented cross-sectional image in (a); (c) the 3D volume element reconstructed from a stack of the binarized and segmented cross-sectional images in (b), with dough matrix transparent and bubbles appearing as yellow-green. Pixel size = 8.75 µm. (For interpretation of the references to color in this figure legend, the reader is referred to the web version of this article.)

($102 \times 102 \times 100$ pixel^3) reconstructed from the center of a stack of one hundred consecutive slices of 2D cross-sectional images is shown in Fig. 1c. When the 2D cross-sectional images are converted to a 3D volume element, bubbles generally appear spherical (Fig. 1c).

In Table 1, the volume fraction of bubbles determined from density measurements ($\phi_{density}$), and the time evolution of the volume fraction of bubbles from X-ray tomography (ϕ_{X-ray}), are presented. Implementation of an objective segmentation technique that does not depend on changes in brightness of an image is essential for correct segmentation during image analysis (Sapirstein, Roller, & Bushuk, 1994; Scanlon & Zghal, 2001), otherwise the density, and thus gas volume fraction, vary by substantial amounts. Since determination of gas volume fraction in the dough via density measurements is easier and more accurate compared to measurements derived from reconstruction of images obtained by methods such as light microscopy (Campbell, Rielly, Fryer, & Sadd, 1991), we calibrated our image segmentation threshold with our density measurements. Accordingly, the choice of appropriate threshold values was such that the gas volume fraction obtained by X-ray microtomography experiments (ϕ_{X-ray}) was identical to the one obtained from dough density measurements ($\phi_{density}$) at the time (15 min) when density measurements were performed.

It can be seen from Table 1 that the volume fraction of gas in wheat flour dough decreases as the time after mixing increases. A decrease in the gas volume fraction with time is not unexpected since the gas in the bubbles in the dough subsample will diffuse to the surrounding atmosphere of the cylindrical plastic container. The change in the gas volume fraction over 126 min was found to be 11% of the original volume. Shimiya and Nakamura (1997) reported approximately three times as much gas loss from their non-yeasted dough samples measured by the change in the ratio of the cross sectional area of bubbles in a dough slice to the total cross sectional area of the slice. Their higher gas loss can be primarily attributed to a much greater surface area available for gas diffusion given that their sample was a thin dough slice, but also to a slightly longer range of aging times (157 min) in their experiments.

In Fig. 2, the BSDs from the two stacks from the three replicate dough subsamples acquired 36 min after the end of mixing are presented. Good correspondence between all six data sets is apparent. For the whole of the size range, the number of bubbles that were detected from each dough stack was in the range of 2800 to 4250, and due to these high numbers, bubbles analyzed will be representative of the bubble population within the whole dough. The number density of bubbles, i.e., number of bubbles per unit volume, ranged from 1350 to 2100 bubbles/mm^3. These number densities are more than an order of magnitude greater than those reported in the literature (Bellido et al., 2006; Campbell et al., 1991; Carlson & Bohlin, 1978; Trinh, Lowe, Campbell, Withers, & Martin, 2013).

As can be seen from Fig. 2, there appear to be a lot of very small bubbles, close to the resolution limit of our images. These bubbles seem to be picked up by our image analysis software due to irregularities in the background of the X-ray images (a salt and pepper like effect). These irregularities were observed within the background of dough matrix, the cylindrical plastic container in which the dough subsamples were placed, and the air. To have absolute confidence in our results, we were able to completely eliminate the salt and pepper like noise when X-ray images were filtered and the bubbles with radii smaller than 16 µm were discounted. Accordingly, when fitting a probability density function to the BSDs extracted from X-ray images, the lower limit of the bubble range used was fixed at 16 µm. By using this lower limit, we realize that bubbles smaller than 16 µm are not contributing to the distribution even though they may well be present in the dough.

Table 1
The gas volume fraction of wheat flour doughs obtained by dough density measurements ($\phi_{density}$) and by X-ray microtomography (ϕ_{X-ray}) as a function of time.

	$\phi_{density} \pm$ sd[a] $= \phi_{X\text{-}ray}$	$\phi_{X\text{-}ray} \pm$ sd[b]			
Time (Min)	15	36	56	148	162
Dough 1	11.16 ± 0.41	10.96 ± 0.04	10.54 ± 0.00	9.64 ± 0.10	9.52 ± 0.26
Dough 2	11.56 ± 0.57	11.36 ± 0.02	11.27 ± 0.01	10.33 ± 0.16	10.25 ± 0.07
Dough 3	10.93 ± 0.42	10.75 ± 0.02	10.01 ± 0.03	9.36 ± 0.17	9.55 ± 0.11

[a] sd = standard deviation, n = 5.
[b] sd = standard deviation (uncertainty reflects the finite increment by which the thresholding can be adjusted), n = 2.

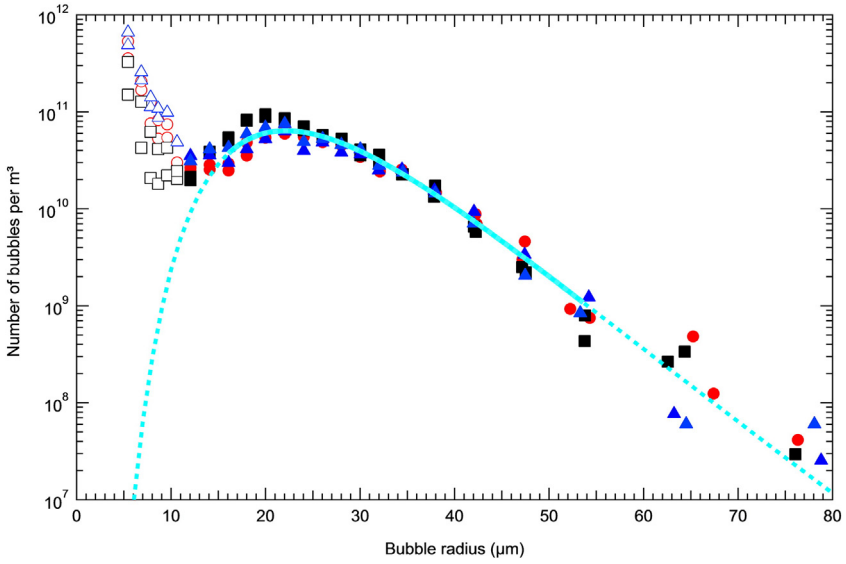

Fig. 2. Bubble size distribution (BSD) of three dough replicates (black squares, red circles and blue triangles) tested 36 min after the end of mixing (two stacks from each dough replicate are represented by the same color). Data points are either denoted as closed (≥10 μm) or open symbols (<10 μm). A lognormal probability density function fitted to the average of the 6 stacks is shown with solid cyan curve (bubble radius range of 16–55 μm), but extended beyond the upper and lower limits (dashed cyan curve). (For interpretation of the references to color in this figure legend, the reader is referred to the web version of this article.)

In dough mixing, the process of iterative subdivision of bubbles into randomly sized bubbles during mixing has a geometric effect on the created bubble sizes, and thus the resulting bubble size distribution in bread dough has been previously characterized as lognormal (Bellido et al., 2006; Shimiya & Nakamura, 1997). Accordingly, a lognormal distribution probability density function (pdf) was used to characterize the experimental BSDs. The pdf is given by:

$$f(R) = \frac{1}{\sqrt{2\pi}\varepsilon R} \exp\left(\frac{-[\ln(R/R_0)]^2}{2\varepsilon^2}\right) \quad (1)$$

where R is bubble radius, R_0 is the median of the lognormal bubble size distribution, and ε is its width.

In fitting the curve to the average of the experimental datasets, the upper limit of the lognormal distribution function was chosen as 55 μm (solid cyan curve in Fig. 2), due to smaller bubble numbers beyond this size. The size range from 16 to 55 μm was used to define all lognormal fits to experimental BSDs. For dough subsamples tested 36 min after the end of mixing, the median radius, R_0, and the width, ε, of the lognormal BSD were 22.1 ± 0.7 μm and 0.31 ± 0.01, respectively. Excellent correspondence between experimental BSDs and the lognormal probability density function fitted to them was found.

As a result of elimination of bubbles with a radius smaller than 16 μm from the BSD, the number density of bubbles in dough subsamples tested 36 min after the end of mixing decreased by 47 ± 12% to 872 ± 134 bubbles/mm^3. This number density is still approximately an order of magnitude greater than what has been previously reported in the literature (Bellido et al., 2006; Campbell et al., 1991; Carlson & Bohlin, 1978; Trinh et al., 2013). The higher bubble number densities in the current study are likely due to the better contrast, higher resolution, and smaller pixel size of the reconstructed X-ray images compared to the ones of Bellido et al. (2006) (10 μm), Campbell et al. (1991) (39 μm), Carlson and Bohlin (1978) (90 μm) and Trinh et al. (2013) (10.8 μm), resulting in better detection of smaller bubbles.

In Fig. 2, even though the lognormal probability density function was fitted to bubbles in the 16 to 55 μm range, bubble radii in the range of 10 to 16 μm are likely to represent real bubbles; the low probability of a contiguous clustering of 7 to 25 voxels is unlikely to be due to noise. We have therefore used closed symbols to denote bubbles with radii between 10 and 16 μm. Bubble radii smaller than or equal to 10 μm signify bubbles formed by less than 7 voxels, where a cluster of 7 voxels represents the minimum number for a 6 point neighboring 3D connectivity criterion. We have therefore used open symbols to represent bubbles with radii smaller than or equal to 10 μm, meaning we have less confidence that they represent real bubbles. Neither bubbles with radii between 10 and 16 μm nor those with radii smaller than or equal to 10 μm were included in the fitting of the BSD equation.

By disregarding bubbles smaller than 16 μm, substantial numbers were not included in our BSD fit. We acknowledge that including them considerably affects the number of bubbles per unit volume; however, these bubbles do not significantly influence the total gas volume fraction of the dough (Trinh et al., 2013). This is also true for bubbles smaller than the resolution of the X-ray microtomography images (bubble volume < 1 voxel) (Turbin-Orger et al., 2012). For doughs tested 36 min after the end of mixing, bubbles smaller than 16 μm contributed less than 0.2% of the total gas in the dough. Here it is important to recognize that if yeasted doughs were being analyzed, bubbles smaller than 16 μm would likely grow due to yeast activity and thus would significantly contribute to the BSD at later stages of the breadmaking process and to the crumb structure of the resulting bread. However, studying the time evolution of non-yeasted doughs is the first step in understanding changes in the bubbly structure of complex soft solids such as bread dough where bubble dynamics is driven only by disproportionation and not also by bubble growth due to yeast activity.

Investigation of the BSD in bread dough goes back to as early as the late 1970s. A variety of techniques including light and electron microscopy, ultrasound, magnetic resonance imaging, bench-top and synchrotron X-ray microtomography have been employed to study the bubbly structure of bread dough. A summary of the literature values reported for the BSD in bread dough is presented in Table 2.

Among the studies that concern bread doughs containing yeast, generally larger bubble sizes have been reported. In a pioneering proving and baking study using X-rays from a synchrotron source with a resolution of 15 μm/pixel, Babin et al. (2006, 2008) reported an arithmetic mean radius of 90 μm a few minutes after kneading. Although Turbin-Orger et al. (2012) followed the approach of Babin et al. (2006), using fast X-rays from a synchrotron source to measure the growth kinetics of bubbles in fermenting dough at a resolution of 5 μm pixels, an initial BSD was not reported. When non-

Table 2
Literature values reported for the mean (or median) radius and the relative standard deviation of the bubble size distribution (BSD) in bread dough.

Reference	Mean or median radius (μm)	Relative standard deviation of the distribution[a]	Method	Time after mixing	Resolution (μm)	Gas volume fraction (%)
With yeast						
Carlson and Bohlin (1978)[b]	57	0.38	LM	NC	90	10
Campbell et al. (1991)[c]	35.5	0.34	LM	NC	39	2.9
Campbell et al. (1991)[c]	44.7	0.53	LM	NC	39	2.8
Whitworth and Alava (1999)	NC	–	CT	During proving	20	5–8
Babin et al. (2006, 2008)	90	–	S-XMT	After kneading	15	10
Without yeast						
Shimiya and Nakamura (1997)[d]	7.5	0.18	LM	3 min	10	4.6[e]
Shimiya and Nakamura (1997)[d]	19	0.16	LM	160 min	10	2.9[e]
Bellido et al. (2006)[d]	50	0.63	B-XMT	90 min	10	7.6
Bellido et al. (2006)[d]	54.7	0.51	B-XMT	90 min	10	9.5
Leroy et al. (2008)[d]	14	0.49	US	53 min	–	12
Leroy et al. (2008)[d]	18	0.46	US	96 min	–	12
Trinh et al. (2013)	60	–	B-XMT	NC	10.8	NC
Current study[d]	22.1	0.32	S-XMT	36 min	8.75	11.0
Current study[d]	27.3	0.32	S-XMT	162 min	8.75	9.8

LM: light microscopy, NC: not communicated, CT: computerized tomography X-ray scanner, S-XMT: X-rays from a synchrotron source, B-XMT: bench-top X-ray microtomography, US: ultrasound.

[a] Relative standard deviation of the distribution is the coefficient of variation (CV). For normal distribution: CV = sd/mean, and for lognormal distribution: $CV = \sqrt{\exp(\varepsilon^2)-1}$ (Limpert, Stahel, & Abbt, 2001).

[b] Mean and standard deviation of the BSD derived according to Campbell et al. (1991)'s empirical formula.

[c] Arithmetic mean and/or standard deviation (sd) of the bubble size distribution.

[d] Median and width (ε) of the lognormal bubble size distribution.

[e] Ratio of the cross sectional area of bubbles to total cross sectional area.

yeasted bread doughs are considered, the use of bench-top X-ray microtomography techniques (Bellido et al., 2006; Trinh et al., 2013) leads to median/mean bubble sizes that are considerably larger than those reported here. Given the capacity of synchrotron X-ray techniques to push the limits of bubble identification in dough, it is likely that greater use of this method, with its improved resolution and contrast, will further reduce the reported values for the median bubble radius in dough, especially if dough is analyzed at very short times after mixing.

3.2. Characterization of the time evolution of dough structure

As time progressed, the peak in the BSD smoothly shifted to higher bubble radius and decreased in magnitude (Fig. 3), while the distribution profile did not change considerably. This shift in BSD peak is indicative of bubble size growth with time due to the diffusion-driven disproportionation of bubbles within the dough (Leroy et al., 2008; Shimiya & Nakamura, 1997). Disproportionation starts right after mixing (van Vliet, 1999) and occurs because gas diffuses from small

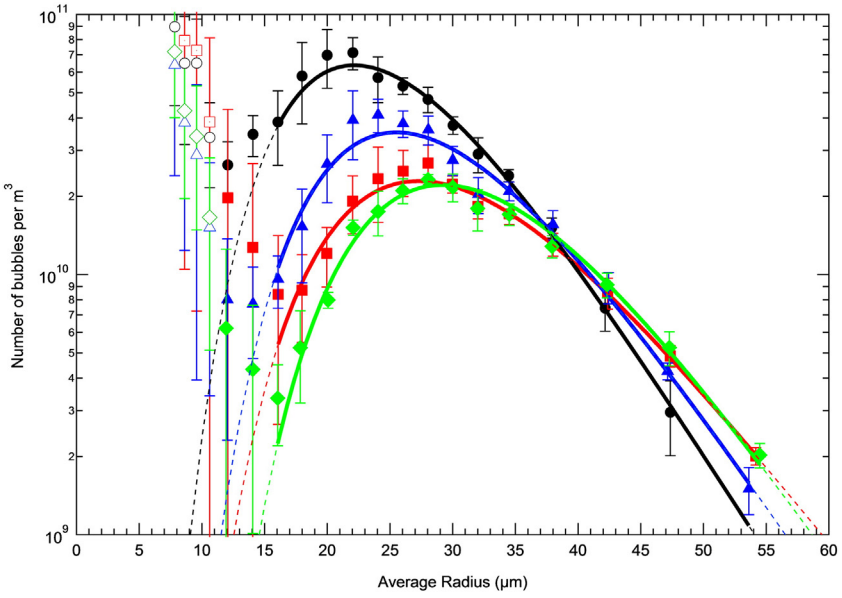

Fig. 3. Time evolution of the bubble size distributions (BSDs) (symbols, black circles: 36 min, blue triangles: 106 min, red squares: 162 min, green diamonds: 190 min) and the lognormal probability density functions (curves with corresponding colors) fitted to them. Lognormal distribution functions are fitted to the averages of 6 stacks for BSDs of 36 ($R^2 = 0.97$) and 162 min ($R^2 = 0.92$) after mixing, and 4 stacks for BSD of 106 ($R^2 = 0.94$)and 190 ($R^2 = 0.97$) min after mixing. Error bars show ±sd of the 6 stacks for 36 and 106 min, and 4 stacks for 162 and 190 min. The fitted lognormal distribution is extended beyond the upper and lower limits of the fitted bubble radius (dashed curves with corresponding colors). (For interpretation of the references to color in this figure legend, the reader is referred to the web version of this article.)

bubbles to adjacent larger ones due to the greater Laplace pressures in the smaller bubbles (Kokelaar et al., 1996; Murray & Ettelaie, 2004; Shimiya & Nakamura, 1997; Shimiya & Yano, 1988).

Over the course of the experiments, the evolution of the BSD was such that the total number of bubbles (R ≥ 16 μm) decreased (Fig. 3), with the decrease being approximately two-fold in 126 min (872 ± 134 bubbles/mm^3 at 36 min to 404 ± 56 bubbles/mm^3 at 162 min after the end of mixing). The decrease in the number density of the bubbles arises because the relatively smaller bubbles shrink and "disappear" (radii become less than 16 μm) since the larger bubbles feed off them. The decrease in the total number of relatively smaller sized bubbles is balanced by growth of the relatively larger sized bubbles, even though there is some overall loss of gas that diffuses from the dough to the surrounding atmosphere (Table 1).

In Fig. 4, the median bubble radius, R_0, of the lognormal distribution function fitted to the BSD is reported as a function of time. It is apparent from the time evolution of R_0 that with increasing time after mixing, the median bubble size grew, verifying the expected changes in bubble sizes within the dough due to disproportionation. The median bubble radius of the BSD increased to 27.3 ± 0.7 μm at 162 min from 22.1 ± 0.7 μm, corresponding to a 2.5% increase in median bubble radius per hour.

It has been reported that during breadmaking, for doughs containing yeast, once the smallest class of bubbles becomes stable or disappears, the growth of the larger bubbles slows down. The size class just next to the smallest class of bubbles does not disappear as quickly as the smallest class did (van Vliet, Janssen, Bloksma, & Walstra, 1992), resulting in a slowing down in the rate of disproportionation for doughs containing yeast. For non-yeasted doughs, Shimiya and Nakamura (1997) also reported that the rate of disproportionation slowed down with time after mixing; over the course of 160 min their median radius was better described by a power law function rather than a linear one. In contrast, in our case, the time evolution of R_0 was better described as a linear increase and a deceleration of the disproportionation rate was not observed.

In Fig. 5, the width, ε, of the lognormal distribution function fitted to the BSD is reported as a function of time. We found that the width changed only slightly during the course of the experiments (ε = 0.31 ± 0.01 at 36 min, 0.31 ± 0.01 at 162 min, and 0.28 ± 0.01 at 190 min). This trend was reported previously for non-yeasted wheat flour doughs, but with much smaller widths; 0.18, 0.18 and 0.16 after 3, 100 and 160 min, respectively (Shimiya & Nakamura, 1997).

A factor that potentially influences our reported results for bubble sizes and their distribution in Figs. 4 and 5 is the apparent deviation from lognormality as time progresses for bubble sizes 10 μm < R ≤ 16 μm (Fig. 3). At these small sizes, we expect few bubbles on the basis of lognormal characterization of the distribution. Nevertheless, significant numbers are observed and these are likely not due to noise. On the basis

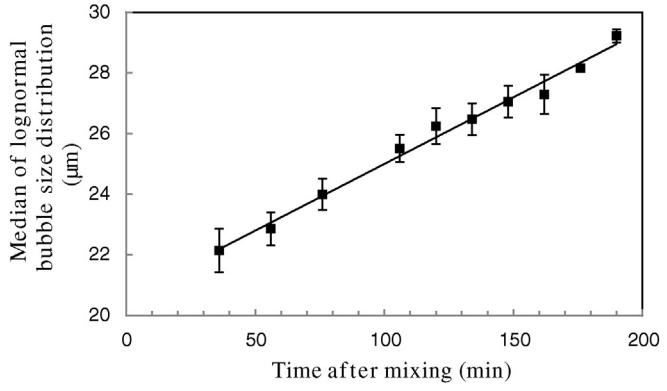

Fig. 4. Time evolution of the median, R_0, of the fitted lognormal bubble size distribution (BSD). Line fitted to time evolution of R_0 has an intercept of 20.6 μm and a slope of 0.044 μm/min. Error bars represent ±sd of 6 stacks for 36, 56, 148 and 162 min, and of 4 stacks for 76, 106, 120, 176 and 190 min.

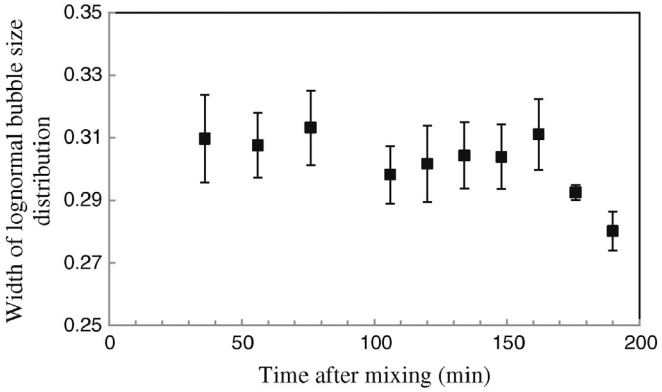

Fig. 5. Time evolution of the width, ε, of the fitted lognormal bubble size distribution (BSD). Error bars represent ±sd of 6 stacks for 36, 56, 148 and 162 min, and of 4 stacks for 76, 106, 120, 176 and 190 min.

of the decrease in size of the smallest bubbles (R ≤ 10 μm) due to disproportionation, a growth in bubble number in the next sizes up (10 μm < R ≤ 16 μm) is expected. As time progresses further, the critical radius – the radius below which all bubbles will shrink (Taylor, 1998) – grows, and intermediate sized bubbles that were initially growing lose gas and shrink, thereby falling into smaller sized bubble bins. A signature of the expected concomitant broadening of the bubble distribution was seen at all times in the bubble size range 10 to 16 μm (Fig. 3).

To provide further evidence of the disproportionation process that accounts for these results, we examined the rate at which bubbles coarsened in the dough. Meinders and van Vliet (2004) studied the rate of change of an ensemble of oil-in-water emulsion droplet sizes as a result of disproportionation. They reported that the coarsening rate of the dispersed phase (oil), ω (m^3/s), is proportional to the diffusion coefficient of the dispersed phase in the bulk phase (water), D (m^2/s), according to the equation:

$$\omega = \frac{dR_c^3}{dt} = \frac{8V_m \sigma D S}{9R_g T \rho} \tag{2}$$

where R_c is the critical radius of the dispersed phase which can be approximated to the number averaged radius (m), t is time (s), V_m is molar volume (m^3/mol), σ is surface tension between the dispersed and bulk phases (N/m), S is solubility of the dispersed phase in the bulk phase (kg/m^3), R_g is the universal gas constant (J/mol·K), T is temperature (K), and ρ is density of the dispersed phase (kg/m^3).

Shimiya and Yano (1988) studied the shrinkage rates of bubbles in doughs at two different temperatures and calculated the apparent diffusion coefficient of air in non-yeasted wheat flour dough as 3.2 ± 1.5×10^{-11} m^2/s at 19 °C and 6.4 ± 2.0×10^{-11} m^2/s at 42 °C. For our wheat flour doughs we used the diffusion coefficient of Shimiya and Yano (1988) at 19 °C and estimated a coarsening rate of ω = 1.7×10^{-19} m^3/s using the solubility of air in water and the molar volume of air in Eq. (2) ($\sigma = 4\times10^{-2}$ N/m, (van Vliet et al., 1992)). This represents a lower bound for the coarsening rate of bubbles in our non-yeasted doughs. We also used the diffusion coefficient of air in water at 25 °C (2×10^{-9}m^2/s) as an upper bound, assuming that the air diffuses from one bubble to another through the dough's free moisture (Chiotellis & Campbell, 2003). From this, we found a coarsening rate of $\omega = 1.1\times10^{-17}$ m^3/s. In comparison, when we calculated the coarsening rate using the median bubble size from our lognormal BSDs, a coarsening rate of $\omega = 1.4\times10^{-18}$ m^3/s was found (ω = 1.5×10^{-18} m^3/s for the number averaged radius of our distributions). Thus, with experimental results lying between the two bounds for the diffusion coefficient for air in dough, we have additional evidence to support disproportionation as the driving force for the changes in bubble sizes in dough that we report here.

4. Conclusions

A high number density of bubbles was found in this study, and this was attributed to the higher resolution of the reconstructed X-ray images obtained by synchrotron radiation. Bubble size distributions in bread dough were very well described by lognormal distribution functions with a median bubble radius of 22.1 ± 0.7 μm (36 min after the end of mixing). Over the course of the next 126 min, the BSD evolved with the total number of the smaller sized bubbles decreasing, ostensibly due to relatively larger bubbles feeding off them. As time progressed after mixing, the median bubble size of the lognormal BSD grew by 2.5% per hour, so that it attained a median bubble size of 27.3 ± 0.7 μm 162 min later. These results confirm transport of gas in the matrix of non-yeasted dough due to disproportionation.

Acknowledgments

The authors would like to acknowledge financial support from the Discovery grants program of the Natural Sciences and Engineering Research Council of Canada. Financial support from the Canadian Light Source Graduate Student Travel Support Program and University of Manitoba Graduate Fellowship for F. K. is also gratefully appreciated. The authors would like to thank Dr. George Belev and Dr. Adam Webb of the Canadian Light Source (Saskatoon, SK) for their technical help and critical discussions. The authors would also like to thank Daiva Daugelaite for her technical help.

References

AACC International (2010). *Approved methods of the American Association of Cereal Chemists* (11th ed.). St. Paul, MN, USA: AACC International. http://dx.doi.org/10.1094/AACCIntMethod-44-15.02.

Babin, P., Della Valle, G., Chiron, H., Cloetens, P., Hoszowska, J., Pernot, P., ... Dendievel, R. (2006). Fast X-ray tomography analysis of bubble growth and foam setting during breadmaking. *Journal of Cereal Science*, *43*(3), 393–397. http://dx.doi.org/10.1016/j.jcs.2005.12.002.

Babin, P., Della Valle, G., Chiron, H., Cloetens, P., Hoszowska, J., Pernot, P., ... Dendievel, R. (2008). In situ fast X-ray tomography study of the evolution of cellular structure in bread dough during proving and baking. In G.M. Campbell, M.G. Scanlon, & L.D. Pyle (Eds.), *Bubbles in food 2: Novelty, health and luxury* (pp. 265–272). St. Paul, MN, USA: Eagan Press.

Babin, P., Della Valle, G., Dendievel, R., Lourdin, D., & Salvo, L. (2007). X-ray tomography study of the cellular structure of extruded starches and its relations with expansion phenomenon and foam mechanical properties. *Carbohydrate Polymers*, *68*(2), 329–340. http://dx.doi.org/10.1016/j.carbpol.2006.12.005.

Baker, J.C., & Mize, M.D. (1941). The origin of the gas cell in bread dough. *Cereal Chemistry*, *18*, 19–34.

Bellido, G.G., Scanlon, M.G., Page, J.H., & Hallgrimsson, B. (2006). The bubble size distribution in wheat flour dough. *Food Research International*, *39*(10), 1058–1066. http://dx.doi.org/10.1016/j.foodres.2006.07.020.

Campbell, G.M., Herrero-Sanchez, R., Payo-Rodriguez, R., & Merchan, M.L. (2001). Measurement of dynamic dough density and effect of surfactants and flour type on aeration during mixing and gas retention during proofing. *Cereal Chemistry*, *78*(3), 272–277.

Campbell, G.M., Rielly, C.D., Fryer, P.J., & Sadd, P.A. (1991). The measurement of bubble size distributions in an opaque food fluid. *Trans IChemE*, *69*, 67–76.

Campbell, G.M., Rielly, C.D., Fryer, P.J., & Sadd, P.A. (1998). Aeration of bread dough during mixing: Effect of mixing dough at reduced pressure. *Cereal Foods World*, *43*(3), 163–167.

Carlson, T., & Bohlin, L. (1978). Free surface energy in the elasticity of wheat flour dough. *Cereal Chemistry*, *55*(4), 539–544.

Chin, N.L., & Campbell, G.M. (2005a). Dough aeration and rheology: Part 1. Effects of mixing speed and headspace pressure on mechanical development of bread dough. *Journal of the Science of Food and Agriculture*, *85*(13), 2184–2193. http://dx.doi.org/10.1002/jsfa.2236.

Chin, N.L., & Campbell, G.M. (2005b). Dough aeration and rheology: Part 2. Effects of flour type, mixing speed and total work input on aeration and rheology of bread dough. *Journal of the Science of Food and Agriculture*, *85*(13), 2194–2202. http://dx.doi.org/10.1002/jsfa.2237.

Chin, N.L., Martin, P.J., & Campbell, G.M. (2005). Dough aeration and rheology: Part 3. Effect of the presence of gas bubbles in bread dough on measured bulk rheology and work input rate. *Journal of the Science of Food and Agriculture*, *85*(13), 2203–2212. http://dx.doi.org/10.1002/jsfa.2238.

Chiotellis, E., & Campbell, G.M. (2003). Proving of bread dough I: Modelling the evolution of the bubble size distribution. *Trans IChemE*, *81*, 194–206.

Falcone, P.M., Baiano, A., Conte, A., Mancini, L., Tromba, G., Zanini, F., & Del Nobile, M.A. (2006). Imaging techniques for the study of food microstructure: A review. *Advances in Food and Nutrition Research*, *51*(06), 205–263. http://dx.doi.org/10.1016/S1043-4526(06)51004-6.

Kaufman, A., Cohen, D., & Yagel, R. (1993). Volume graphics. *Computer*, *26*(7), 51–64.

Kokelaar, J.J., van Vliet, T., & Prins, A. (1996). Strain hardening properties and extensibility of flour and gluten doughs in relation to breadmaking performance. *Journal of Cereal Science*, *24*(3), 199–214. http://dx.doi.org/10.1006/jcrs.1996.0053.

Koksel, F., & Scanlon, M.G. (2012). Effects of composition on dough development and air entrainment in doughs made from gluten-starch blends. *Journal of Cereal Science*, *56*(2), 445–450. http://dx.doi.org/10.1016/j.jcs.2012.05.013.

Koksel, F., Strybulevych, A., Page, J.H., & Scanlon, M.G. (2014). Ultrasonic characterization of unyeasted bread dough of different sodium chloride concentrations. *Cereal Chemistry*, *91*(4), 327–332. http://dx.doi.org/10.1094/CCHEM-10-13-0206-CESI.

Leroy, V., Fan, Y., Strybulevych, A., Bellido, G.G., Page, J.H., & Scanlon, M.G. (2008). Investigating the bubble size distribution in dough using ultrasound. In G.M. Campbell, M.G. Scanlon, & D.L. Pyle (Eds.), *Bubbles in food 2: Novelty, health and luxury* (pp. 51–60). St. Paul, MN, USA: Eagan Press.

Limpert, E., Stahel, W.A., & Abbt, M. (2001). Log-normal distributions across the sciences: Keys and clues. *Bioscience*, *51*(5), 341–352. http://dx.doi.org/10.1641/0006-3568(2001)051[0341:LNDATS]2.0.CO;2.

Meinders, M.B.J., & van Vliet, T. (2004). The role of interfacial rheological properties on Ostwald ripening in emulsions. *Advances in Colloid and Interface Science*, *108–109*, 119–126. http://dx.doi.org/10.1016/j.cis.2003.10.005.

Murray, B.S., & Ettelaie, R. (2004). Foam stability: Proteins and nanoparticles. *Current Opinion in Colloid & Interface Science*, *9*(5), 314–320. http://dx.doi.org/10.1016/j.cocis.2004.09.004.

Sapirstein, H.D., Roller, R., & Bushuk, W. (1994). Instrumental measurement of bread crumb grain by digital image analysis. *Cereal Chemistry*, *71*(4), 383–391.

Scanlon, M.G., & Zghal, M.C. (2001). Bread properties and crumb structure. *Food Research International*, *34*(10), 841–864. http://dx.doi.org/10.1016/S0963-9969(01)00109-0.

Scanlon, M.G., Elmehdi, H.M., Leroy, V., & Page, J.H. (2008). Using ultrasound to probe nucleation and growth of bubbles in bread dough and to examine the resulting cellular structure of bread crumb. In G.M. Campbell, M.G. Scanlon, & D.L. Pyle (Eds.), *Bubbles in food 2: Novelty, health and luxury* (pp. 217–230). St. Paul, MN, USA: Eagan Press.

Scanlon, M.G., Page, J.H., Leroy, V., Fan, Y., Elmehdi, H.M., Kiefte, A., & Mehta, K.L. (2011). Using low frequency ultrasound to evaluate the properties of wheat flour doughs. In R.N. Chibbar, & J.E. Dexter (Eds.), *Proceedings of the 4th International Wheat Quality Conference* (pp. 271–282). Jodhpur, India: Agrobios International.

Shimiya, Y., & Nakamura, K. (1997). Changes in size of gas cells in dough and bread during breadmaking and calculation of critical size of gas cells that expand. *Journal of Texture Studies*, *28*(3), 273–288. http://dx.doi.org/10.1111/j.1745-4603.1997.tb00117.x.

Shimiya, Y., & Yano, T. (1988). Rates of shrinkage and growth of air bubbles entrained in wheat flour dough. *Agricultural and Biological Chemistry*, *52*(11), 2879–2883.

Strybulevych, A., Leroy, V., Shum, A.L., Koksel, H.F., Scanlon, M.G., & Page, J.H. (2012). Use of an ultrasonic reflectance technique to examine bubble size changes in dough. *IOP Conference Series: Materials Science and Engineering*, *42*. (pp. 1–4). http://dx.doi.org/10.1088/1757-899X/42/1/012037.

Taylor, P. (1998). Ostwald ripening in emulsions. *Advances in Colloid and Interface Science*, *75*(2), 107–163. http://dx.doi.org/10.1016/S0001-8686(98)00035-9.

Trater, A.M., Alavi, S., & Rizvi, S.S.H. (2005). Use of non-invasive X-ray microtomography for characterizing microstructure of extruded biopolymer foams. *Food Research International*, *38*(6), 709–719. http://dx.doi.org/10.1016/j.foodres.2005.01.006.

Trinh, L., Lowe, T., Campbell, G.M., Withers, P.J., & Martin, P.J. (2013). Bread dough aeration dynamics during pressure step-change mixing: Studies by X-ray tomography, dough density and population balance modelling. *Chemical Engineering Science*, *101*, 470–477. http://dx.doi.org/10.1016/j.ces.2013.06.053.

Turbin-Orger, A., Babin, P., Boller, E., Chaunier, L., Chiron, H., Della Valle, G., ... Salvo, L. (2015). Growth and setting of gas bubbles in a viscoelastic matrix imaged by X-ray microtomography: The evolution of cellular structure in fermenting wheat flour dough. *Soft Matter*, *11*, 3373–3384. http://dx.doi.org/10.1039/C5SM00100E.

Turbin-Orger, A., Boller, E., Chaunier, L., Chiron, H., Della Valle, G., & Réguerre, A. -L. (2012). Kinetics of bubble growth in wheat flour dough during proofing studied by computed X-ray micro-tomography. *Journal of Cereal Science*, *56*(3), 676–683. http://dx.doi.org/10.1016/j.jcs.2012.08.008.

van Vliet, T. (1999). Physical factors determining gas cell stability in a dough during bread making. In G.M. Campbell, C. Webb, S. S. Pandiella, & K. Niranjan (Eds.), *Bubbles in food* (pp. 121–127). St. Paul, MN, USA: Eagan Press.

van Vliet, T., Janssen, A.M., Bloksma, A.H., & Walstra, P. (1992). Strain hardening of dough as a requirement for gas retention. *Journal of Texture Studies*, *23*, 439–460. http://dx.doi.org/10.1111/j.1745-4603.1992.tb00033.x.

Vu, R.H., Rangayyan, R.M., Deglint, H.J., & Boag, G.S. (2007). Segmentation and analysis of neuroblastoma. *Journal of the Franklin Institute*, *344*(3–4), 257–284. http://dx.doi.org/10.1016/j.jfranklin.2006.11.002.

Whitworth, M.B., & Alava, J.M. (1999). Imaging and measurement of bubbles in bread doughs. In G.M. Campbell, C. Webb, S.S. Pandiella, & K. Niranjan (Eds.), *Bubbles in food* (pp. 221–231). St. Paul, MN, USA: Eagan Press.